Journal of Magnetic Resonance **151,** 332–338 (2001)
doi:10.1006/jmre.2001.2375, available online at http://www.idealibrary.com on IDEAL®

COMMUNICATIONS

Accurate Measurement of Small Spin–Spin Couplings in Partially Aligned Molecules Using a Novel *J*-Mismatch Compensated Spin-State-Selection Filter

Bernhard Brutscher

Institut de Biologie Structurale, Jean-Pierre Ebel C.N.R.S.—C.E.A., 41, rue Jules Horowitz, 38027 Grenoble Cedex, France

Received February 21, 2001; revised May 4, 2001; published online July 6, 2001

The accurate measurement of small spin–spin coupling constants in macromolecules dissolved in a liquid crystalline phase is important in the context of molecular structure investigation by modern liquid state NMR. A new spin-state-selection filter, DIPSAP, is presented with significantly reduced sensitivity to *J*-mismatch of the filter delays compared to previously proposed pulse sequences. DIPSAP presents an attractive new approach for the accurate measurement of small spin–spin coupling constants in molecules dissolved in anisotropic solution. Application to the measurement of ^{15}N–^{13}C′ and ^{1}H^{N}–^{13}C′ coupling constants in the peptide planes of ^{13}C, ^{15}N labeled proteins demonstrates the high accuracy obtained by a DIPSAP-based experiment.

Key Words: **liquid state NMR; spin-state selection; molecular alignment, residual dipolar coupling; TROSY.**

Recently it has been demonstrated (*1*) that incomplete directional averaging of macromolecules in liquid crystalline media, e.g., bicelles (*2, 3*), filamentous phage (*4, 5*), purple membrane fragments (*6*), alcohol mixtures (*7*), strained gels (*8*), or cellulose crystallites (*9*), allows the measurement of residual dipolar couplings (RDC) while retaining conditions essential for high resolution liquid state NMR. Because of the partial alignment of the solute molecule in the anisotropic liquid-crystalline phase, the effective spin–spin coupling is the sum of a scalar and a dipolar contribution: $J_{IS}^{eff} = J_{IS}^{sc} + D_{IS}^{res}$. The RDC constant D_{IS}^{res} depends on the orientation of the internuclear I–S vector with respect to the molecular alignment frame, and therefore provides unique orientational long-range constraints for the structure determination of macromolecules. So far, RDC data have been successfully used to define the relative orientation of molecular domains (*10, 11*), to validate structural homology models (*12–14*), or to improve the accuracy of structures determined by NMR (*15–17*). Very recently it has been shown for the first time that an accurate three-dimensional model of the protein backbone can be built from RDC data alone, provided the data are complete, accurate, and precise enough (*18, 19*). In the present context high accuracy means the absence of systematic error in the RDC measurements, whereas high precision indicates a small standard deviation of a measured RDC from repeated experiments. As the magnitude of the residual dipolar couplings is determined by the degree of alignment, it is desirable to use samples with a (relatively) high degree of alignment, allowing more precise measurements of the coupling constants. Molecular alignment resulting in residual dipolar couplings of up to $|^{1}D_{NH}^{res}| \cong 40$ Hz for the ^{15}N–^{1}H backbone vector has indeed been obtained for proteins dissolved in liquid-crystalline phases. Broadening of the ^{1}H resonances in such partially aligned samples due to unresolved ^{1}H–^{1}H RDC can be partly avoided by deuteration of most of the nonexchangeable protons in the molecule (*20*), or by homonuclear adiabatic decoupling (*21*).

The separation of two doublet components into different subspectra provides a simple approach of measuring small coupling constants, and it has also become important in the context of transverse relaxation optimized spectroscopy (TROSY) (*22*), where selection of the slowly relaxing doublet component provides increased resolution and sensitivity in heteronuclear correlation experiments of macromolecules. In recent years, several techniques have been proposed to achieve spin-state selection (or separation) using only nonselective radiofrequency (rf) pulses. First the S^3 family of sequences, with S^3E (*23*) achieving spin-state-selective excitation, and S^3CT (*24*) performing a spin-state-selective π-rotation. Two successive S^3CT building blocks are needed for a spin-state-selective coherence transfer (*22, 25*). Alternatively, spin-state selection can simply be realized by the addition and subtraction of two spectra, one showing in-phase peak doublets and the other showing anti-phase peak doublets. This technique has become known as IPAP (*26, 27*). All of these filter sequences are prone to artifacts resulting in spurious peaks detected at the position of the suppressed doublet components, thus limiting the accuracy of measurements of small spin–spin couplings by these techniques. The origin of these artifacts are mainly differential spin relaxation between the different detected coherence transfer pathways and *J*-mismatch.

1090-7807/01 $35.00

Relaxation-induced artifacts and techniques for their suppression have been discussed previously for S^3E (*28*), S^3CT (*29, 30*), and IPAP (*26, 27*). Because the filter delay Δ must be tuned to match the coupling constant J_{IS}^{eff}, $\Delta = 1/4J_{IS}^{eff}$ in the case of S^3E, and $\Delta = 1/2J_{IS}^{eff}$ for IPAP and S^3CT, these filters are also sensitive to variations in the size of the coupling constant J_{IS}^{eff} (*26, 31*). The large range of effective one-bond coupling constants observed for partially aligned samples may thus induce significant systematic errors in the coupling constant measurements. Here a new spin-state-selective filter is presented, which is insensitive to *J*-mismatch over a wide range of effective coupling constants. This pulse sequence element is easily implemented in any heteronuclear NMR experiment to separate the individual components of a peak doublet into subspectra. The method is demonstrated for the measurement of small ${}^2J_{C'HN}^{eff}$ and ${}^1J_{C'N}^{eff}$ coupling constants in ^{13}C,^{15}N labeled proteins.

The *J*-mismatch compensated spin-state-selection filter is shown in Fig. 1A. This new filter sequence is an extension of the IPAP technique, where spin-state selection is achieved by the combination of an in-phase and an anti-phase spectrum. In the case of *J*-mismatch, however, the two spectra do not have the same intensity and a residual peak is detected at the position of the suppressed doublet component (*26, 27*). A *J*-mismatch compensated version of IPAP is obtained by recording two in-phase spectra, one with a higher and one with a lower intensity than the corresponding anti-phase spectrum. We refer to this new sequence as DIPSAP (double-in-phase-single-anti-phase) filter. In practice, the three spectra are obtained by setting the filter delayΔ to $\Delta = 1/\overline{J_{IS}}$ (instead of $\Delta = 1/2\overline{J_{IS}}$ for IPAP) and the delay ε and phase φ as follows: (a) $\varepsilon = \Delta/4, \varphi = x$, (b) $\varepsilon = 0, \varphi = x$, and (c) $\varepsilon = \Delta/8, \varphi = y$. For the spectrum (a) J_{IS} coupling evolution during the filter is completely refocused, whereas for the spectra (b) and (c) J_{IS} coupling evolution occurs for an effective time period of Δ and $\Delta/2$, respectively. Assuming the spin system is prepared as I_z magnetization prior to the filter, the coherence transfer pathways and transfer amplitudes for the three experiments are given by: (a) $I_z \rightarrow I_z\mathrm{R}(\Delta)$, (b) $I_z \rightarrow I_z\mathrm{R}(\Delta)\cos(\pi J_{IS}\Delta)$, and (c) $I_z \rightarrow 2I_zS_z\mathrm{R}(\Delta)\sin(\pi J_{IS}\Delta/2)$, where $\mathrm{R}(\Delta)$ denotes the signal decay as a result of spin relaxation and pulse imperfections. Alternatively, the filter may act on initial $2I_zS_z$ spin order, and the coherence transfer pathways are simply obtained by interchanging I_z and $2I_zS_z$ in the expressions given above. Coupling constants between a spin I (or an additional spin K) and a passive spin S are then measured in a subsequent incremented time period t_1. To avoid artifacts as discussed above, the filter has been designed in a way that signal loss during the sequence due to pulse imperfections and auto- and cross-correlated relaxation is identical for all three experiments. In particular, CSA–dipolar cross correlated relaxation is removed by the 180° pulse applied to the S spins at half of the filter delay. It is advantageous to place the filter sequence directly prior to the t_1 evolution to avoid differential relaxation during the time period between the filter and the spin coupling evolution.

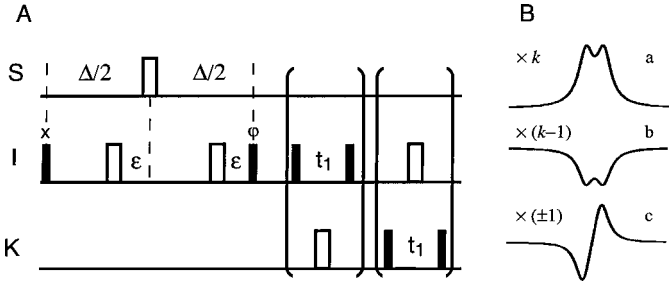

FIG. 1. (A) Pulse sequence of the DIPSAP spin-state-selection filter based on a J_{IS}^{eff} coupling evolution. Three data sets need to be recorded with the following settings: (a) $\varepsilon = \Delta/4$, $\varphi = x$, (b) $\varepsilon = 0$, $\varphi = x$, and (c) $\varepsilon = \Delta/8$, $\varphi = y$. Couplings to the passive spin S are then measured in a subsequent t_1 evolution period either for the spin I or an additional spin K. (B) Typical spectra obtained by the use of an DIPSAP filter. In the case of J-mismatch, the two in-phase spectra have a (a) higher and a (b) lower intensity than the corresponding (c) anti-phase spectrum. The two spin-state-separated subspectra are obtained by the linear combination $k\mathrm{a} + (k-1)\mathrm{b} \pm \mathrm{c}$ with the optimized scaling factor $k = 0.73$.

The different sensitivity of the recorded spectra to *J*-mismatch becomes more visible when the amplitude factors given above are expressed as a function of the relative *J*-mismatch factor $(J_{IS}^{eff} - \overline{J_{IS}})/\overline{J_{IS}}$. The normalized intensity of the three spectra is then given by: (a) 1, (b) $-\cos(\pi(J_{IS}^{eff} - \overline{J_{IS}})/\overline{J_{IS}})$, and (c) $\cos(\frac{\pi}{2}(J_{IS}^{eff} - \overline{J_{IS}})/\overline{J_{IS}})$. Although the two spectra (b) and (c) show both a cosine dependence on *J*-mismatch, the signal intensity of the in-phase spectrum (b) decreases faster with increasing *J*-mismatch than the intensity of the anti-phase spectrum (c). In addition, the two in-phase spectra, (a) and (b) are of opposite phase, as illustrated in Fig. 1B. The separation of the α and β doublet components in two subspectra by the linear combination $k\mathrm{a} + (k-1)\mathrm{b} \pm \mathrm{c}$, with k the scaling factor between the two in-phase spectra, should thus allow to reduce the sensitivity of the filter to *J*-mismatch. The intensity ratio of the residual over the selected doublet component as a function of the relative *J*-mismatch is given by

$$\frac{I^{res}}{I^{sel}} = \frac{\left(k + (1-k)\cos\left(\pi\frac{J_{IS}^{eff} - \overline{J_{IS}}}{\overline{J_{IS}}}\right) - \cos\left(\frac{\pi}{2}\frac{J_{IS}^{eff} - \overline{J_{IS}}}{\overline{J_{IS}}}\right)\right)}{\left(k + (1-k)\cos\left(\pi\frac{J_{IS}^{eff} - \overline{J_{IS}}}{\overline{J_{IS}}}\right) + \cos\left(\frac{\pi}{2}\frac{J_{IS}^{eff} - \overline{J_{IS}}}{\overline{J_{IS}}}\right)\right)}. \quad [1]$$

In order to evaluate the performance of DIPSAP in the presence of *J*-mismatch we expand Eq. [1] into a Taylor series yielding the following expression:

$$\frac{I^{res}}{I^{sel}} = \frac{4k-3}{16}\left(\frac{J_{IS}^{eff} - \overline{J_{IS}}}{\overline{J_{IS}}}\right)^2 + \sum_{n=4}^{\infty} a_n\left(\frac{J_{IS}^{eff} - \overline{J_{IS}}}{\overline{J_{IS}}}\right)^n. \quad [2]$$

For $k = 0.75$, J-mismatch compensation up to third order is obtained by the DIPSAP filter, whereas the S^3E and IPAP (S^3CT)

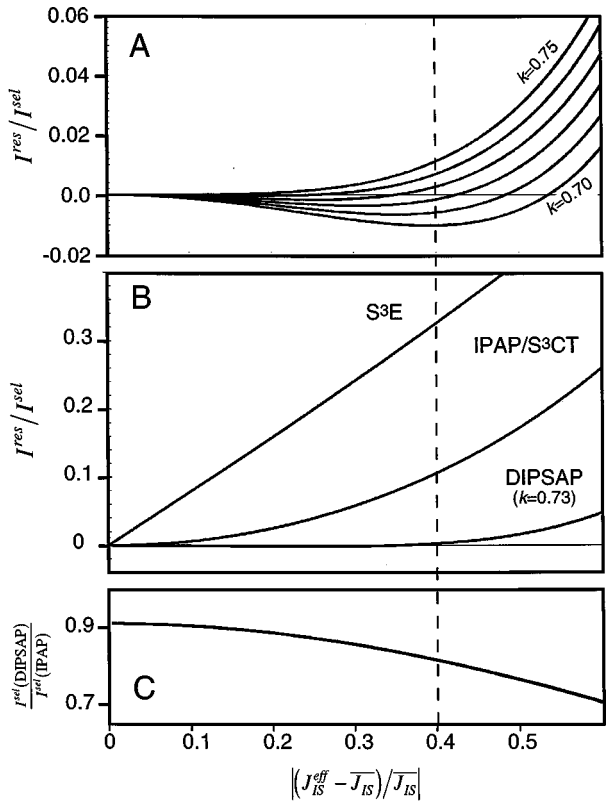

FIG. 2. (A) J-mismatch profiles of DIPSAP calculated for different k values ranging from 0.70 to 0.75 in steps of 0.01. The I^{res}/I^{sel} ratio is given by Eq. [1]. (B) J-mismatch profiles of different spin-state-selection filters: S^3E, IPAP, S^3CT, and DIPSAP ($k = 0.73$). The I^{res}/I^{sel} ratios for S^3E are given by

$$\tan\left(\frac{\pi}{4}\frac{J_{IS}^{eff}-\overline{J_{IS}}}{\overline{J_{IS}}}\right)$$

and for IPAP and S^3CT by

$$\left(1-\cos\left(\frac{\pi}{2}\frac{J_{IS}^{eff}-\overline{J_{IS}}}{\overline{J_{IS}}}\right)\right)\Big/\left(1+\cos\left(\frac{\pi}{2}\frac{J_{IS}^{eff}-\overline{J_{IS}}}{\overline{J_{IS}}}\right)\right).$$

(C) Intensity ratio of a doublet peak selected by a DIPSAP and an IPAP filter sequence as a function of J-mismatch, $\frac{I^{sel}(\text{DIPSAP})}{I^{sel}(\text{IPAP})} = \frac{2\sqrt{3}}{3\sqrt{0.73^2+0.27^2+1}} \times \left(0.73+0.27\cos(\pi J^{mis})+\cos\left(\frac{\pi}{2}J^{mis}\right)\right)/\left(1+\cos\left(\frac{\pi}{2}J^{mis}\right)\right)$, with $J^{mis} = (J_{IS}^{eff}-\overline{J_{IS}})/\overline{J_{IS}}$. Relaxation effects are neglected for the calculation.

filters achieve only compensation up to zero and first order, respectively. Starting from the analytically obtained value of $k = 0.75$, the performance of the DIPSAP filter can be further optimized by slightly adjusting the scaling factor k taking into account the actual range of J_{IS}^{eff} values. J-mismatch profiles calculated for DIPSAP with different k values ranging from 0.75 to 0.70 are shown in Fig. 2A. For a range of effective J couplings $|(J_{IS}^{eff}-\overline{J_{IS}})/\overline{J_{IS}}| \le 0.4$, the best profile is obtained with $k = 0.73$. Inside this range the intensity of the residual doublet component is below 0.2% of the intensity of the selected doublet component ($I^{res}/I^{sel} \le 0.002$). This J-mismatch compensated filter band width should be sufficient for most applications as it covers the largest variations of coupling constants observed for macromolecules dissolved in a liquid-crystalline phase. If necessary, this effective J-mismatch compensated filter band width may be further increased by accepting slightly higher residual intensities, e.g., for a tolerable residual intensity of 1.0% ($I^{res}/I^{sel} \le 0.01$) the optimal scaling factor is $k = 0.70$ resulting in a filter band width of $|(J_{IS}^{eff}-\overline{J_{IS}})/\overline{J_{IS}}| \le 0.58$. The J-mismatch profiles calculated for DIPSAP ($k = 0.73$), S^3E, IPAP, and S^3CT are plotted in Fig. 2B. Although the IPAP and S^3CT methods are considerably less sensitive to variations in J_{IS}^{eff} than S^3E, only DIPSAP yields clean separation of the two doublet components inside the range $|(J_{IS}^{eff}-\overline{J_{IS}})/\overline{J_{IS}}| \le 0.4$.

A drawback of the DIPSAP filter (with respect to IPAP) is the slightly reduced signal to noise ratio obtained by the experiment, which affects the precision of the coupling constant measurements but not their accuracy. If the filter cannot be concatenated with a coherence transfer period, the longer filter delay ($\Delta = 1/\overline{J_{IS}}$ instead of $\Delta = 1/2\overline{J_{IS}}$) induces additional signal loss due to spin relaxation. The signal decay $R(\Delta)$ depends on the transverse relaxation rates of the involved coherences and thus on the size of the molecule. The signal to noise ratio is further decreased by the recording and linear combination of two different in-phase spectra. The origin of this sensitivity loss is twofold. First, the unequal numerical weighting of the recorded in-phase spectra slightly reduces the signal to noise ratio even in the absence of J-mismatch. For optimal sensitivity, numerical scaling could be avoided by adjustment of the scan number of the individual experiments (*32*). In practice, however, the use of an equal scan number and numerical readjustment of the experiments is more convenient, as the scan number in multidimensional experiments is mainly dictated by the available experimental time and the required phase cycle. Second, in the case of J-mismatch the additional in-phase spectra, exclusively recorded for DIPSAP, has a lower intensity than the two other spectra, also recorded for IPAP. The simulated ratio of peak intensities measured with DIPSAP ($k = 0.73$) and IPAP is plotted in Fig. 2C as a function of J-mismatch. The curve has been calculated neglecting relaxation effects and normalized for equal experimental time and noise level. The sensitivity loss varies between 9% for exact match of the effective spin–spin coupling by the filter delay and 18% for a J-mismatch $|(J_{IS}^{eff}-\overline{J_{IS}})/\overline{J_{IS}}| = 0.4$.

In order to estimate the systematic error induced in the coupling constant measurements by using IPAP to separate the doublet components, we have calculated the apparent line splitting as a function of the coupling constant J_{IS}^{eff} and the line width $\Delta\nu$. Line shapes were assumed to be Gaussian, which is a more realistic approximation than Lorentzian for the line shapes observed in multidimensional experiments using standard apodisation functions. The peak positions were determined as the points of maximum intensity. The expected error in the measured J couplings for a I^{res}/I^{sel} ratio of 0.1, which corresponds to a J-mismatch of $|(J_{IS}^{eff}-\overline{J_{IS}})/\overline{J_{IS}}| = 0.39$ for IPAP, is plotted in Fig. 3 as a

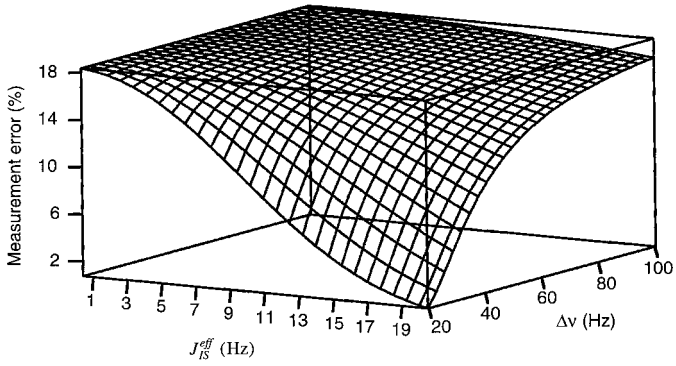

FIG. 3. Systematic error in the measurement of coupling constants using IPAP or S^3CT spin-state selection for a J-mismatch of $|(J_{IS}^{eff} - \overline{J_{IS}})/\overline{J_{IS}}| = 0.39$ as a function of the coupling constant J_{IS}^{eff} and the line width $\Delta\nu$. The line shapes were assumed to be Gaussian for the simulation.

function of J_{IS}^{eff} and $\Delta\upsilon$. The error increases with increasing line width and decreasing coupling constant. For small couplings ($J_{IS}^{eff}/\Delta\upsilon \ll 1$) the error reaches a maximum of about 18%. This error is significantly higher than the precision obtained for the measurement of spin–spin coupling constants in ^{13}C/^{15}N labeled proteins or nucleic acids. The use of DIPSAP instead of IPAP (or S^3E) eliminates this additional source of measurement error, and therefore provides an attractive alternative for the accurate measurement of small coupling constants in partially aligned molecules.

As an example of practical interest we implemented the new DIPSAP filter sequence in 3D HNCO-type experiments designed for the measurement of the small coupling constants $^2J_{C'HN}^{eff}$ and $^1J_{C'N}^{eff}$ in the peptide planes of proteins (*33, 34*). The pulse sequences for the HNCO-J$_{C'H}$ and HNCO-J$_{C'N}$ experiments are displayed in Figs. 4A and 4B, respectively. The coherence transfer pathway for the two experiments can be described by

$$\begin{aligned} {}^1H^N \xrightarrow{{}^1J_{NH}^{eff}} {}^{15}N \xrightarrow{{}^1J_{NC}^{eff}} {}^{13}C'(t_1) \\ \xrightarrow{{}^1J_{NC}^{eff}} {}^{15}N(t_2) \xrightarrow{{}^1J_{NH}^{eff}} {}^1H^N(t_3), \end{aligned} \qquad [3]$$

where the couplings involved in the transfer steps are indicated above the arrows and t_{1-3} are acquisition times. The major difference with previously proposed sequences is the insertion of a DIPSAP filter element highlighted in gray in Fig. 4. In both pulse sequences, the DIPSAP filter uses the large one-bond $^1J_{NH}^{eff}$ coupling for spin-state selection along the ^{13}C′ frequency dimension. In the HNCO-$J_{C'H}$ experiment (Fig. 4A) the DIPSAP filter acts on ^{15}N transverse coherence and can be concatenated with the ^{15}N → ^{13}C′ transfer step to reduce relaxation-induced signal loss. In the HNCO-$J_{C'N}$ experiment (Fig. 4B) the DIPSAP filter acts on ^{1}H^N transverse coherence, which is created after the ^{15}N → ^{13}C′ transfer step, and thus it induces an additional delay of $1/\overline{J_{NH}} \cong 11$ ms. At the end of the DIPSAP filter in the HNCO-$J_{C'H}$ (HNCO-$J_{C'N}$) experiment, the state of the spin system is described by the product operators $4H_z^N N_z C_z'$ for (a) and (b), and $2N_z C_z'$ ($2H_z^N C_z'$) for (c). During the following t_1 period the ^{13}C′ spins are frequency labeled in the absence of ^{1}H (^{15}N) decoupling. Three data sets (a–c) are recorded in an interleaved manner, yielding cross peaks with in-phase (a, b) and anti-phase (c) $J_{C'H}$ ($J_{C'N}$) splittings in the C′ frequency dimension. After appropriate linear combination (0.73a − 0.27b ± c) two three-dimensional subspectra are obtained with cross peaks at $(\omega_{C'} + \pi^2 J_{C'HN}^{eff}, \omega_N, \omega_H)$ and $(\omega_{C'} - \pi^2 J_{C'HN}^{eff}, \omega_N, \omega_H)$ for the HNCO-$J_{C'H}$ experiment, and $(\omega_{C'} + \pi^1 J_{C'N}^{eff}, \omega_N, \omega_H)$ and $(\omega_{C'} - \pi^1 J_{C'N}^{eff}, \omega_N, \omega_H)$ for the HNCO-$J_{C'N}$ experiment. The small $^2J_{C'HN}^{eff}$ and $^1J_{C'N}^{eff}$ coupling constants can then be obtained from a precise measurement of peak positions along the ^{13}C frequency dimension.

Some additional points of interest concerning the pulse sequences of Fig. 4 are discussed in the following. The efficiency of each individual transfer step in the HNCO experiment depends on the J-mismatch. After an INEPT-type transfer the signal intensity is proportional to

$$\cos\left(\frac{\pi}{2}\frac{(J_{IS}^{eff} - \overline{J_{IS}})}{\overline{J_{IS}}}\right).$$

For a J-mismatch as large as $|(J_{IS}^{eff} - \overline{J_{IS}})/\overline{J_{IS}}| = 0.4$ this results in an additional signal loss of about 20% per transfer step, an amount which may be affordable for this intrinsically very sensitive experiment. Much higher degrees of molecular alignment are certainly not desirable as the advantage of larger RDC is counterbalanced by the important signal loss during transfer and filter delays induced by the J-mismatch. In order to limit the number of transfer steps sensitive to J-mismatch in the HNCO pulses sequences, refocusing of the $^1J_{NH}^{eff}$ coupling during the subsequent ^{15}N → ^{13}C transfer step combined with composite ^{1}H decoupling is not applied here. Note that in the absence of ^{1}H decoupling, relaxation loss during ^{15}N transverse spin evolution will be reduced by CSA(^{15}N)–dipolar (^{1}H–^{15}N) cross correlated relaxation, the so called TROSY effect (*22, 35*). This is the case between time points a and b, and c and d for the two experiments depicted in Fig. 4. In the presented pulse sequences, however, the TROSY effect is suppressed during the ^{15}N and ^{1}H frequency editing periods (t_2, t_3), providing the highest sensitivity for moderately sized proteins. For application to large (per)deuterated proteins, where the slowly relaxing ^{15}N doublet component is reduced beyond detection at time point *e*, the sensitivity of the experiment can be further increased by simply omitting the 180° ^{1}H pulse (marked by a star in Fig. 4) and the composite ^{15}N decoupling during detection. The cross peaks will then be shifted by πJ_{NH}^{eff} in the ω_2 and ω_3 frequency dimensions.

To demonstrate the performance of the new experiments in the case of J-mismatch, we recorded 2D spectra (ω_1, ω_3) on a test sample of ^{13}C, ^{15}N labeled ubiquitin in isotropic solution.

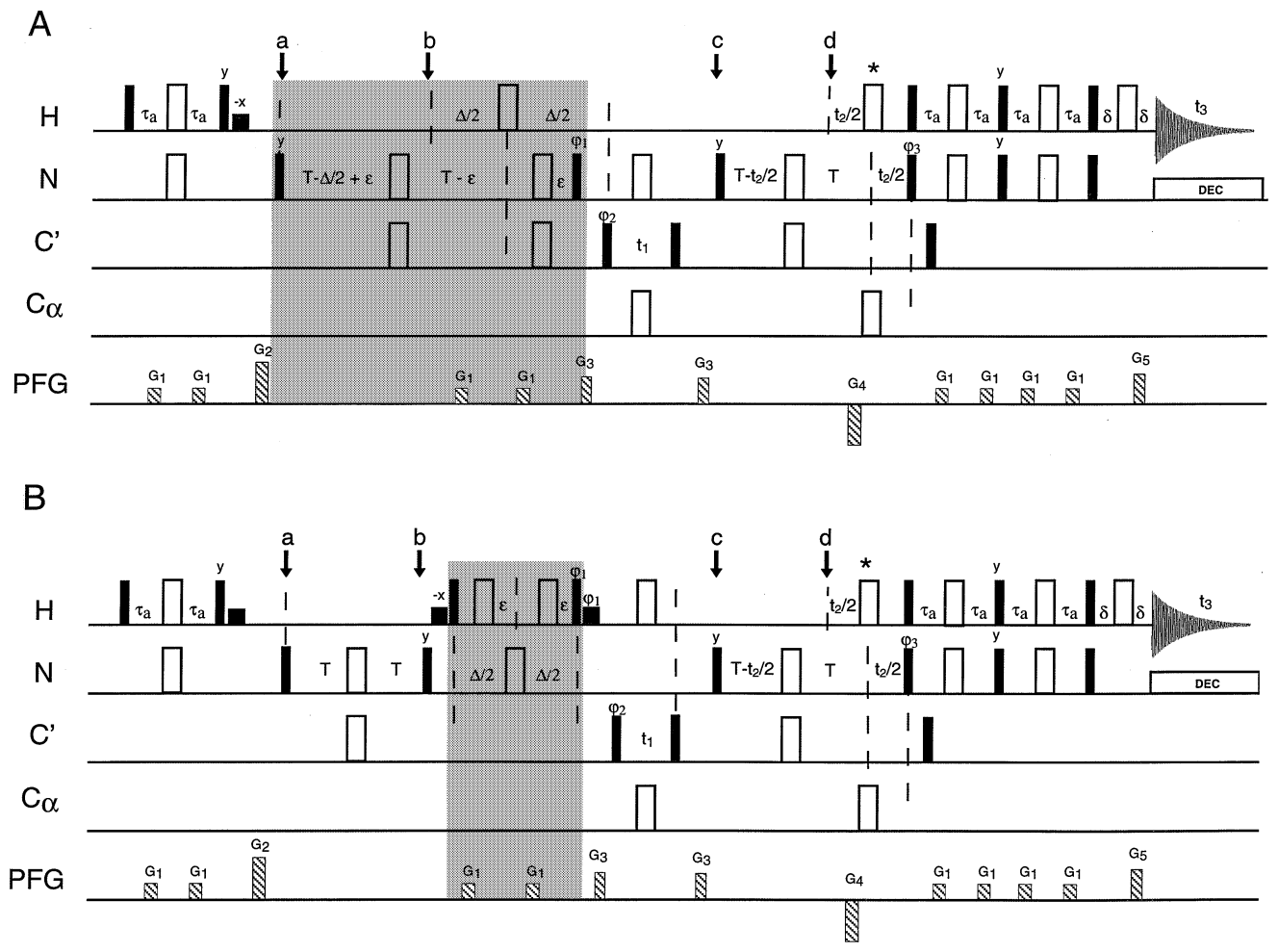

FIG. 4. Pulse sequences for (A) 3D HNCO-$J_{C'H}$ and (B) 3D HNCO-$J_{C'N}$ experiments including a J-mismatch compensated DIPSAP filter (gray shaded) for spin-state selection. In (A) the DIPSAP filter is concatenated with the $^{15}N \rightarrow {}^{13}C'$ transfer period. All rf pulses are applied along the x axis unless indicated and 90° and 180°RF pulses are represented by filled and open bars, respectively. The ^{13}C pulses applied to C′ have the shape of the center lobe of a $\sin x/x$ function, whereas the C^{α} pulses are applied with a rectangular shape and field strength of $\Delta/\sqrt{15}$ (90°) and $\Delta/\sqrt{3}$ (180°), where Δ is the separation in Hz between the centers of the C^{α} and C′ chemical shift regions. The transfer and filter delays were adjusted to $\tau_a = 1/4\overline{J_{NH}}$, $T = 1/4\overline{J_{NC'}}$, and $\Delta = 1/\overline{J_{NH}}$. Three data sets need to be recorded with the delay ε and phase φ adjusted to: (a) $\varepsilon = \Delta/4$, $\varphi_1 = x$, (b) $\varepsilon = 0$, $\varphi_1 = x$, and (c) $\varepsilon = \Delta/8$, $\varphi_1 = y$. Pulsed field gradients G_1, G_2, G_3, G_4, and G_5 are applied along the z axis (PFG_z) with a gradient strength of approximately 20 G/cm and lengths ranging from 100 to 1000 μs, followed by a recovery delay of 100 μs. The relative duration of G_4 and G_5 are given by the gyromagnetic ratios of ^1H and ^{15}N as $G_4/G_5 = \gamma_H/\gamma_N$. A two-step phase cycle was applied with $\varphi_2 = x, -x$ and the receiver phase $\varphi_{rec} = x, -x$. Quadrature detection in the ^{13}C dimension (t_1) is achieved by incrementing the phase φ_2 according to the STATES-TPPI method, while in the ^{15}N dimension (t_2) sensitivity enhanced quadrature detection is used, where for each t_2 increment φ_3 is increased by 180° and the sign of G_4 is inverted. The last $^{13}C'$ 90° is a purge pulse required to suppress undesired coherence transfer pathways (*33*).

First, the experiments were performed by setting the DIPSAP filter delay to $\Delta = 1/J_{NH}^{sc}$ with the average scalar coupling $J_{NH}^{sc} = 92$ Hz. The experiments were then repeated by changing the filter delay to $\Delta = 1.4/J_{NH}^{sc}$ resulting in a J-mismatch of $|(J_{IS}^{eff} - \overline{J}_{IS})/\overline{J}_{IS}| = 0.4$. For comparison, additional spectra were recorded by replacing the DIPSAP filter element by a standard IPAP filter. Again two data sets were recorded, one with exact match of the filter delay and one with a J-mismatch $|(J_{IS}^{eff} - \overline{J}_{IS})/\overline{J}_{IS}| = 0.4$. A small part of the recorded 2D spectra showing two $^{13}C'$–$^1H^N$ correlation peaks from the peptide planes G53–R54 and I61–Q62 are plotted in Figs. 5A–5D (HNCO–$J_{C'H}$) and Figs. 5E–5H (HNCO–$J_{C'N}$). For simplicity, the α and β subspectra are superimposed on the same plot with a relative shift of ±0.02 ppm along the ^1H dimension to visually separate the two peaks. As expected, the signal to noise ratio in the spectra recorded with an IPAP filter is slightly higher than in the corresponding spectra obtained with a DIPSAP filter. Peak positions were determined by extracting 1D traces along the ^{13}C dimension and performing a nonlinear least-square fitting of the peak assuming a Gaussian shape. The ^{13}C line width at half height was $\Delta\upsilon \approx 25$ Hz and the average precision of the measured coupling constants was ±0.1 Hz for $^2J_{C'HN}^{eff}$ and ±0.3 Hz for $^1J_{C'N}^{eff}$. For both couplings, the use of a DIPSAP filter yields accurate results within the experimental error for a J-mismatch

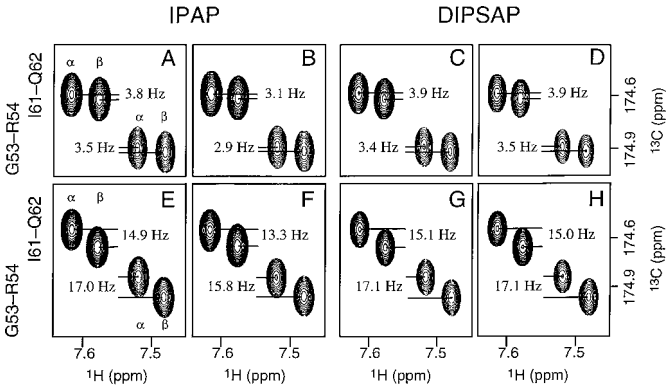

FIG. 5. Small region of the 2D correlation spectra recorded with the HNCO-$J_{C'H}$ experiment of Fig. 4A (A–D) and the HNCO-$J_{C'N}$ experiment of Fig. 4B (E–H) using different filter techniques and delay tuning: (A and E) IPAP and no J-mismatch, (B and F) IPAP with J-mismatch of 0.4, (C and G) DIPSAP and no J-mismatch, (D and H) DIPSAP with J-mismatch of 0.4. The α and β subspectra are superposed with a shift along the ^{1}H dimension of $+0.02$ and -0.02 ppm, respectively. All spectra were recorded on a 2-mM sample of ^{13}C, ^{15}N labeled ubiquitin (90% H_2O, 10% D_2O, pH 4.7, 27°C) at 600 MHz ^{1}H frequency. Data sets of 100(^{13}C) × 512(^{1}H) complex points were recorded for spectral widths of 2260 Hz (^{13}C) and 9000 Hz (^{1}H) in an experimental time of 4 h per experiment. Before Fourier transformation, the time domain data were multiplied by a squared cosine function in t_1 and t_3, and zero-filled to final matrices of 1024 × 1024 complex points.

of $|(J_{IS}^{eff} - \overline{J}_{IS})/\overline{J}_{IS}| = 0.4$, whereas the coupling constants are systematically underestimated when using an IPAP filter in the case of J-mismatch. Absolute (and relative) measurement errors of 0.5–0.7 Hz (16–18%) for $^2J_{C'HN}^{eff}$, and 1.2–1.7 Hz (8–11%) for $^1J_{C'N}^{eff}$ are obtained for $|(J_{IS}^{eff} - \overline{J}_{IS})/\overline{J}_{IS}| = 0.4$. The systematic errors are several times larger than the experimental precision obtained from these experiments. These conclusions should also be valid for larger proteins in anisotropic solution, where spectra of high signal to noise ratio can be recorded in a reasonable experimental time ($\leq$3 days).

In summary, a novel J-mismatch compensated spin-state-selection filter, DIPSAP, is presented which allows clean separation of doublet lines in subspectra. Application of DIPSAP to the measurement of $^2J_{C'HN}^{eff}$ and $^1J_{C'N}^{eff}$ coupling constants in the peptide planes of proteins is shown. The experimental results are in good agreement with simulations (Fig. 3), and confirm the superiority of DIPSAP over previously proposed filter techniques in the case of J-mismatch for the accurate measurement of spin–spin couplings which are small compared to the line width. Large variations of coupling constants from one molecular site to the other are obtained when residual dipolar couplings, observed for molecules dissolved in an anisotropic medium, add to the effective spin–spin couplings. As the line widths increase with the size of the molecules we expect that the new DIPSAP filter will be especially attractive for the measurement of RDC constants in partially aligned macromolecules, where high accuracy is required for their use as restraints in RDC-based structure calculation protocols (19).

ACKNOWLEDGMENTS

The author thanks M. Blackledge, J. Boisbouvier, and J.-P. Simorre for stimulating discussion and careful reading of the manuscript. This work was supported by the Commisariat à l'Energie Atomique, the Centre National de la Recherche Scientifique (France), and Molecular Simulations Inc. (San Diego, CA).

REFERENCES

1. N. Tjandra and A. Bax, Direct measurement of distances and angles in biomolecules by NMR in a dilute liquid crystalline medium, *Science* **278,** 1111–1114 (1997).
2. M. Ottiger and A. Bax, Characterisation of magnetically oriented phospholipid micelles for measurement of dipolar couplings in macromolecules, *J. Biomol. NMR.* **12,** 361–372 (1998).
3. H. Wang, M. Eberstadt, E. T. Olejniczak, R. P. Meadows, and S. W. Fesik, A liquid crystalline medium for measuring residual dipolar couplings over a wide range of temperatures, *J. Biomol. NMR.* **12,** 443–446 (1998).
4. G. M. Clore, M. R. Starich, and A. M. Gronenborn, Measurement of residual dipolar couplings of macromolecules aligned in the nematic phase of a colloidal suspension of rod-shaped viruses, *J. Am. Chem. Soc.* **120,** 10,571–10,572 (1998).
5. M. R. Hansen, L. Mueller, and A. Pardi, Tunable alignment of nucleic acids and proteins by filamentous phage provides a new method for obtaining dipolar coupling distance and angle constraints, *Nat. Struct. Biol.* **5,** 1065–1074 (1998).
6. J. Saas, F. Cordier, A. Hoffmann, M. Rogowski, A. Cousin, J. G. Omichinski, H. Löwen, and S. Grzesiek, Purple membrane induced alignment of biological macromolecules in the magnetic field, *J. Am. Chem. Soc.* **121,** 2047–2055 (1999).
7. M. Rückert and G. Otting, Alignment of biological macromolecules in novel nonionic crystalline media for NMR experiments, *J. Am. Chem. Soc.* **122,** 7793–7797 (2000).
8. R. Tycko, F. J. Blanco, and Y. Ishii, Alignment of biopolymers in strained gels: A new way to create detectable dipole–dipole couplings in high-resolution biomolecular NMR, *J. Am. Chem. Soc.* **122,** 9340–9341 (2000).
9. K. Flemming, D. Gray, S. Prasannan, and S. Matthews, Cellulose crystallites: A new and robust liquid crystalline medium for the measurement of residual dipolar couplings, *J. Am. Chem. Soc.* **122,** 5224–5225 (2000).
10. M. W. F. Fischer, J. A. Losonczi, J. L. Weaver, and J. H. Prestegard, Domain orientation and dynamics in multidomain proteins from residual dipolar couplings, *Biochemistry* **38,** 9013–9022 (1999).
11. N. R. Skrynnikov, N. K. Goto, D. Yang, W.-Y. Choy, J. R. Tolman, G. A. Mueller, and L. E. Kay, Orienting domains in proteins using dipolar couplings measured by liquid-state NMR: Differences in solution and crystal forms of maltodextrin binding protein loaded with β-cyclodextrine, *J. Mol. Biol.* **295,** 1265–1273 (2000).
12. A. Annila, H. Aito, E. Thulin, and T. Drakenberg, Recognition of protein folds via dipolar couplings, *J. Biomol. NMR.* **14,** 223–230 (1999).
13. J. Meiler, W. Peti, and C. Griesinger, DipoCoup: A versatile program for 3D-structure homology comparison based on residual dipolar couplings and pseudocontact shifts, *J. Biomol. NMR.* **17,** 283–294 (2000).
14. J. J. Chou, S. Li, and A. Bax, Study of conformational rearrangement and refinement of structural homology models by the use of heteronuclear dipolar couplings, *J. Biomol. NMR.* **18,** 217–227 (2000).
15. N. Tjandra, J. G. Omichinski, A. M. Gronenborn, G. M. Clore, and A. Bax, Use of ^{1}H–^{15}N and ^{1}H–^{13}C couplings in the structure determination of magnetically oriented macromolecules in solution, *Nature Struct. Biol.* **4,** 732–738 (1997).

16. G. M. Clore, M. R. Starich, C. A. Bewley, M. Cai, and J. Kuszewski, Impact of residual dipolar couplings on the accuracy of NMR structures determined from a minimal number of NOE restraints, *J. Am. Chem. Soc.* **121,** 6513–6514 (1999).
17. G. A. Mueller, W. Y. Choy, N. R. Skrynnikov, and L. E. Kay, A method for incorporating dipolar couplings into structure calculations in cases of (near) axial symmetry of alignment, *J. Biomol. NMR.* **18,** 183–188 (2000).
18. F. Delaglio, G. Kontaxis, and A. Bax, Protein structure determination using molecular fragment replacement and NMR dipolar couplings, *J. Am. Chem. Soc*. **122,** 2142–2143 (2000).
19. J. C. Hus, D. Marion, and M. Blackledge, Determination of protein backbone structure using only residual dipolar couplings, *J. Am. Chem. Soc*. **123,** 1541–1542 (2001).
20. K. H. Gardner and L. E. Kay, The use of ^{2}H, ^{13}C, ^{15}N Multidimensional NMR to study the structure and dynamics of proteins, *Annu. Rev. Biophys. Biomol. Struct.* **27,** 357–406 (1998).
21. C. W. Vander Kooi, E. Kupce, E. R. P. Zuiderweg, and M. Pellecchia, Line narrowing in spectra of proteins dissolved in dilute liquid crystalline phase by band-selective adiabatic decoupling: Application to $^{1}H^{N}$–^{15}N dipolar coupling measurements, *J. Biomol. NMR.* **15,** 335–338 (1999).
22. K. Pervushin, R. Riek, G. Wider, and K. Wüthrich, Attenuated T_2 relaxation by mutual cancellation of dipole–dipole coupling and chemical shift anisotropy indicates an avenue to NMR structures of very large biological macromolecules in solution, *Proc. Natl. Acad. Sci. USA.* **94,** 12,366–12,371 (1997).
23. A. Meissner, J. Ø. Duus, and O. W. Sørensen, Spin-state-selective excitation. Application for E-COSY-type measurement of J_{HH} coupling constants, *J. Magn. Reson*. **128,** 92–97 (1997).
24. M. D. Sørensen, A. Meissner, and O. W. Sørensen, Spin-state-selective coherence transfer via intermediate states of two-spin coherence in IS spin systems: Application to E.COSY-type measurements of J coupling constants, *J. Biomol. NMR.* **10,** 181–186 (1997).
25. A. Meissner, T. Schulte-Herbrüggen, J. Briand, and O. W. Sørensen, Double spin-state-selective coherence transfer. Application for two-dimensional selection of multiplet components with long transverse relaxation times, *Mol. Phys.* **95,** 1137–1142 (1998).
26. M. Ottiger, F. Delaglio, and A. Bax, Measurement of J and dipolar couplings from simplified two-dimensional NMR spectra, *J. Magn. Reson*. **131,** 373–378 (1998).
27. P. Anderson, J. Weigelt, and G. Otting, Spin-state selection filters for the measurement of heteronuclear one-bond coupling constants, *J. Biomol. NMR*. **12,** 435–441 (1998).
28. A. Meissner, T. Schulte-Herbrüggen, and O. W. Sørensen, Relaxation artifacts and their suppression in multidimensional E.COSY-type NMR experiments for measurement of J coupling constants in ^{13}C- or ^{15}N-labeled proteins, *J. Am. Chem. Soc*. **120,** 7989–7990 (1998).
29. T. Schulte-Herbrüggen and O. W. Sørensen, Clean TROSY: Compensation for relaxation-induced artifacts, *J. Magn. Reson*. **144,** 123–128 (2000).
30. C. Kojima and M. Kainosho, Simple suppression of spurious peaks in TROSY experiments, *J. Magn. Reson*. **143,** 417–422 (2000).
31. P. Permi, S. Heikkinen, I. Kilpeläinen, and A. Annila, Measurement of $^{1}J_{NC'}$ and $^{2}J_{HC'}$ couplings from spin-state-selective two-dimensional correlation spectrum, *J. Magn. Reson.* **140,** 32–40 (1999).
32. O. W. Sørensen, Sensitivity optimization in subspectral editing, *J. Magn. Reson*. **57,** 506–512 (1984).
33. D. Yang, R. A. Venters, G. A. Mueller, W. Y. Choy, and L. E. Kay, TROSY-based HNCO pulse sequences for the measurement of ^{1}HN-^{15}N, ^{15}N-^{13}CO, ^{1}HN-^{13}CO, ^{13}CO-$^{13}C^{\alpha}$ and ^{1}HN-$^{13}C^{\alpha}$ dipolar couplings in ^{15}N, ^{13}C, ^{2}H-labeled proteins, *J. Biomol. NMR*. **14,** 333–343 (1999).
34. P. Permi, P. R. Rosevear, and A. Annila, A set of HNCO-based experiments for the measurement of residual dipolar couplings in ^{15}N, ^{13}C, (^{2}H)-labeled proteins, *J. Biomol. NMR*. **17,** 43–54 (2000).
35. B. Brutscher, Principles and applications of cross-correlated relaxation in biomolecules, *Concepts in Magn. Reson*. **12,** 207–229 (2000).